Chemosphere 254 (2020) 126859

Contents lists available at ScienceDirect

Chemosphere

journal homepage: www.elsevier.com/locate/chemosphere

Organic complexation of U(VI) in reducing soils at a natural analogue site: Implications for uranium transport

Adam J. Fuller [a, 1], Peter Leary [b], Neil D. Gray [b], Helena S. Davies [c], J. Frederick W. Mosselmans [d], Filipa Cox [c], Clare H. Robinson [c], Jon K. Pittman [c], Clare M. McCann [b], Michael Muir [e], Margaret C. Graham [e], Satoshi Utsunomiya [f], William R. Bower [a, g], Katherine Morris [c], Samuel Shaw [c], Pieter Bots [c, 2], Francis R. Livens [a, c], Gareth T.W. Law [a, g, *]

[a] Centre for Radiochemistry Research, Department of Chemistry, The University of Manchester, Manchester, M13 9PL, UK
[b] School of Natural and Environmental Sciences, Newcastle University, Newcastle, NE1 7RU, UK
[c] Research Centre for Radwaste Disposal, and Williamson Centre for Molecular Environmental Science, Department of Earth and Environmental Sciences, The University of Manchester, Manchester, M13 9PL, UK
[d] Diamond Light Source, Harwell Science and Innovation Campus, Didcot, Oxfordshire, OX11 0DE, UK
[e] School of Geoscience, University of Edinburgh, Edinburgh, EH9 3FF, UK
[f] School of Chemistry, Kyushu University, 744 Motooka, Nishi-ku, Fukuoka, 819-0395, Japan
[g] Radiochemistry Unit, Department of Chemistry, The University of Helsinki, 00014, Finland

HIGHLIGHTS

- Up to 1600 mg kg^{-1} $U(VI)_{(s)}$ retained in Needle's Eye soils by organic complexation.
- Uranyl-organic complexes stable under Fe(III)-reducing conditions.
- U(VI) reduced to non-crystalline U(IV) under sulfate reducing/methanogenic conditions.
- U hard to remobilise from Needle's Eye soil.

ARTICLE INFO

Article history:
Received 29 January 2020
Received in revised form
7 April 2020
Accepted 19 April 2020
Available online 28 April 2020

Handling Editor: Martine Leermakers

Keywords:
Uranium
Radionuclide biogeochemistry
Natural analogue site
Needle's eye

ABSTRACT

Understanding the long-term fate, stability, and bioavailability of uranium (U) in the environment is important for the management of nuclear legacy sites and radioactive wastes. Analysis of U behavior at natural analogue sites permits evaluation of U biogeochemistry under conditions more representative of long-term equilibrium. Here, we have used bulk geochemical and microbial community analysis of soils, coupled with X-ray absorption spectroscopy and μ-focus X-ray fluorescence mapping, to gain a mechanistic understanding of the fate of U transported into an organic-rich soil from a pitchblende vein at the UK Needle's Eye Natural Analogue site. U is highly enriched in the Needle's Eye soils (~1600 mg kg^{-1}). We show that this enrichment is largely controlled by U(VI) complexation with soil organic matter and not U(VI) bioreduction. Instead, organic-associated U(VI) seems to remain stable under microbially-mediated Fe(III)-reducing conditions. U(IV) (as non-crystalline U(IV)) was only observed at greater depths at the site (>25 cm); the soil here was comparatively mineral-rich, organic-poor, and sulfate-reducing/methanogenic. Furthermore, nanocrystalline UO_2, an alternative product of U(VI) reduction in soils, was not observed at the site, and U did not appear to be associated with Fe-bearing minerals. Organic-

* Corresponding author. Radiochemistry Unit, Department of Chemistry, The University of Helsinki, 00014, Finland.
E-mail address: gareth.law@helsinki.fi (G.T.W. Law).
[1] Current address: Galsons Sciences, 5 Grosvenor House, Melton Road, Oakham, Rutland, LE15 6AX, UK.
[2] Current address: Civil and Environmental Engineering, University of Strathclyde, Glasgow, G11 XQ, UK.

https://doi.org/10.1016/j.chemosphere.2020.126859

rich soils appear to have the potential to impede U groundwater transport, irrespective of ambient redox conditions.

1. Introduction

The management of radioactively contaminated land and the geological disposal of radioactive wastes present wide-ranging environmental and socioeconomic challenges. Tackling these challenges in an efficient and safe manner requires a comprehensive understanding of radionuclide behavior in the geo- and biosphere. Uranium (U) is a common contaminant in the environment and its toxicity poses a hazard to human and ecosystem health. U is also a major constituent of radioactive wastes destined for geological disposal and given its long half-life ($^{238}U = 4.46 \times 10^9$ years, $^{235}U = 7.03 \times 10^8$ years), some U will inevitably be released from waste packages into the geosphere.

In oxic groundwater at circumneutral pH, U(VI) dominates as the UO_2^{2+} ion; uranyl carbonate and phosphate complexes can also form depending on groundwater conditions (Choppin et al., 2002; Newsome et al., 2014). Whilst reasonably soluble, U(VI) can be retained in soils through a range of processes. Sorption of U(VI) onto a variety of mineral surfaces (especially Fe oxy(hydr)oxides) has been documented (e.g. Hsi and Langmuir, 1985; Catalano and Brown, 2005; Sherman et al., 2008), but it is often reversible, especially at pH > 7 (e.g. Sherman et al., 2008; Alam and Cheng, 2014). This reversibility leaves sorbed U(VI) potentially mobile in the geosphere. Reflecting this issue, a range of studies have focused on U(VI) reduction to sparingly soluble U(IV). U(VI) reduction in the environment occurs via biotic, abiotic, and coupled biotic-abiotic pathways, with microbes playing an important, often dominant role (e.g. see the reviews of Bargar et al., 2013 and Newsome et al., 2014). Early work in pure culture experiments showed that U(VI) enzymatic reduction (bioreduction) led to the precipitation of crystalline UO_2 (Lovley et al., 1991; Lovley and Phillips, 1992). More recently, bioreduction has also been shown to produce non-crystalline U(IV) species (e.g. Bernier-Latmani et al., 2010; Alessi et al., 2012, 2014). Non-crystalline U(IV) formation is particularly favored in the presence of phosphate and sulfate (Fletcher et al., 2010; Boyanov et al., 2011; Ray et al., 2011; Stylo et al., 2013; Alessi et al., 2014; Morin et al., 2016). Further, it is also known to complex with cell exudates and organic matter (Alessi et al., 2014; Bone et al., 2017). Although poorly soluble under reducing conditions, both non-crystalline U(IV) and UO_2 undergo oxidative remobilisation due to reaction with O_2 and NO_3^- (Moon et al., 2007; Cerrato et al., 2013), with non-crystalline U(IV) suggested to be more labile (Sharp et al., 2011). U(V) species have been documented in pure culture bioreduction experiments (e.g. Renshaw et al., 2005; Vettese et al., 2020) but they are unstable with respect to disproportionation. However, when U(VI) is reduced abiotically commensurate with the formation of Fe(II)-bearing minerals, U(V) can be stabilized in the Fe mineral lattice (Pidchenko et al., 2017; Roberts et al., 2017). Clearly, to understand uranium's longer-term fate in soils and other environments, it is crucial to understand its speciation.

In this work, we investigate the mechanisms of U retention in an organic-rich soil. Waterlogged organic soils found in peat bogs and wetlands are known to hyper-accumulate U via a range of mechanisms including U complexation with organics and mineral phases, and reduction of U(VI) to poorly soluble U(IV) (e.g. Wang et al., 2013; Cumberland et al., 2016; Kaplan et al., 2016; Koster van Groos et al., 2016). As such, wetlands may offer a passive remediation approach to limit U migration in the geosphere (e.g. Groza et al., 2010). Retention of U by organic matter in soils is likely dominated by its complexation on carboxylate groups (Regenspurg et al., 2010; Mikutta et al., 2016), with U known to form monodentate, bidentate, and bridging complexes with humic acids in constrained studies (Denecke et al., 1997, 1998 A and B). However, the potential mobility and bioavailability of organically complexed U, and its redox stability, are only starting to be understood (e.g. Cumberland et al., 2016, 2018 A and B). Of note, mobile U(IV)-bearing colloids have also been observed in wetland sediments (Wang et al., 2013).

Here we extend current understanding of U biogeochemistry and availability in organic-rich soils by investigating the mechanism and strength of U retention in samples taken from the Needle's Eye natural analogue site, UK (Hooker, 1991; Jamet et al., 1993). This site is contaminated with U that is sourced from a local pitchblende vein. Natural analogue sites permit study of radionuclide behavior at realistic concentrations in 'real' environments. In particular, areas of U mineralization are well established as analogues for geological disposal facilities (International Atomic Energy Agency, 1989). Whatever the origin of the radionuclides, they have generally been present for decades or much longer, and these long equilibration times provide a unique research opportunity which cannot be replicated in the laboratory.

The Needle's Eye site geology and hydrogeology has been described by Mackenzie et al. (1991) and Jamet et al. (1993). Briefly, oxidizing groundwater percolates through the local country rock which contains pitchblende bearing veins and other mineralizations (e.g. As, Co). Weathering of these deposits results in groundwater enriched in U and its daughter radionuclides. The U-bearing water then flows outward from a cliff into a water-logged, organic-rich, soil layer (~1 m deep), which is underlain by a narrow band of clay (~10 cm), and coarse gravel (Mackenzie et al., 1991). The U-bearing groundwater flows (5–10 m) through the soil towards the near-by coast, however ~80–90% of the supplied U becomes associated with the solids in the organic rich soil layer (Mackenzie et al., 1991). This soil layer is estimated to have accumulated over the last 5000 years, and has been described as anoxic (Mackenzie et al., 1991; Jamet et al., 1993). Based on field survey data and geochemical modelling, U retention in Needle's Eye soils was attributed to U association with Fe and Mn oxy(hydr)oxides and U(VI) reduction and precipitation of UO_2 (Mackenzie et al., 1991; Jamet et al., 1993) in the site's reducing soils. The potential role of U complexation with organic matter at the site has also been discussed (e.g. Jamet et al., 1993), but this could not be evaluated at the time. Given the above, Needle's Eye presents a natural analogue site where one can better understand U biogeochemistry, transport, and fate in organic-rich soils. Sites with organic rich soils could receive U released from nuclear waste disposal facilities, or from leakages/spills at nuclear mega-sites.

In this work, we re-examined the Needle's Eye site to test whether the alternative mechanisms of U retention recently described in the literature (i.e. organic complexation and/or non-crystalline U(IV) formation) play an important role in controlling U mobility at Needle's Eye. Further, we sought to examine how U speciation at Needle's Eye impacts U availability/leachability from the soil. Given the long equilbration time of U at the Needle's Eye

site and the tendency for organic-rich soils to be heavily reducing, we hypothesized that U at Needle's Eye would ultimately be sequestered in these soils as nanocrystalline UO_2. Indeed, laboratory work has shown that this phase can dominate U(IV) speciation in reducing sediment systems given time (Stylo et al., 2013; Newsome et al., 2015; Bower et al., 2019).

2. Materials and methods

2.1. Site description and field sampling

Two cores (~40 cm in length) were collected from the same area of the Needle's Eye site (roughly 50 cm apart) close to the pitchblende vein (see Fig. S1). For sampling, 50 cm Perspex (ID 10 cm) core tubes were inserted into the soil; they were then capped at the top to form a vacuum, removed, and capped at the bottom. After extraction, the headspace was opened, flushed with O_2-free Ar, and then resealed. The cores were quickly (~3 h) returned to the laboratory for sectioning. One core was sectioned at 1 cm resolution under oxic conditions and freeze-dried to provide samples for bulk soil analysis. A second core was sectioned at the same resolution under an O_2-free N_2 atmosphere to preserve the redox state of the samples. These sections were then immediately frozen at −80 °C under O_2-free N_2 until further analysis. The bottom 5–10 cm of each core was not used for sediment analysis (except for microbial ecology) in order to minimize the risk of any U oxidation via contact with the atmosphere. An additional core from the same location was collected for resin embedding, thin sectioning, and synchrotron μ-focus X-ray fluorescence mapping (see Appendix section S1 for further detail). Groundwater/porewater was also sampled at 5 cm depth intervals at Needle's Eye using *in-situ* 'PushPoint' syringe samplers (M.H.E Products, USA). Details of this sampling and analysis are provided in the Appendix (section S2). Finally, a "control" core was collected ~100 m away (laterally) from the area impacted by the Needle's Eye pitchblende vein. This core was sectioned under oxic conditions.

2.2. Geochemical analysis

The Needle's Eye core sectioned under a normal atmosphere was prepared for solid phase elemental analysis by X-ray fluorescence (XRF). The soil samples were freeze-dried, homogenized, and finely ground in an agate ball mill. Samples were then pressed into a pellet with wax binder and analyzed on a Thermo ARL 9400 XRF, with data normalised for C content. Water content and organic matter and total carbon content were determined by loss on ignition. 2 g of field-moist soil from each depth was heated to 105 °C to determine water content, 375 °C for organic matter content, and 950 °C for total carbon. Samples were cooled in a desiccator and reweighed after each temperature point. A sub-sample of the Needle's Eye core sectioned under N_2 was used for measurement of the solid phase 0.5 mol L^{-1} HCl extractable Fe(II/III) ratio (Lovley and Phillips, 1987). Additional sub-samples of this core were used for microbial community analysis, sequential extractions, and bulk X-ray absorption spectroscopy (XAS). Finally, soil samples from the "control" core were processed in a similar way (see above) and were analyzed for U content by XRF.

2.3. Uranium extractions

Sequential extractions were performed to probe the dominant soil phase responsible for U retention in the Needle's Eye soil. The sequential extraction followed the method of Vandenhove et al. (2014). Briefly, the reagents and targeted fractions were: 0.5 mol L^{-1} $MgCl_2$, for the 'exchangeable phase'; 1 mol L^{-1} sodium acetate, for 'carbonates'; 0.1 mol L^{-1} $NH_2OH.HCl$, for 'oxides'; 30% H_2O_2, for 'organics'; and concentrated *aqua regia* for any 'residual' material (from Zimmerman and Weindorf, 2010). Full details concerning the extraction conditions and method are given in the Appendix (section S3 and Table S1). Of note, we cannot rule out that the 0.1 mol L^{-1} $NH_2OH.HCl$ step may reduce U(VI) that is associated with the soils, which in turn could impact the U extracted in this, and following steps.

To further test whether the exchangeability of the U from the soil was kinetically hindered, 0.500 ± 0.005g samples of soil from 15 and 30 cm depth were suspended in 5 mL of 0.1 M $MgCl_2$ and shaken for one month with samples collected at 30 min, 1 h, 24 h, 1 week, and 1 month. This was completed under an O_2-free atmosphere and also from tubes frequently opened to a normal atmosphere to test for potential impacts of U(IV) oxidative remobilisation (with O_2).

2.4. Microbial community analysis

DNA was extracted using a FastDNA Spin Kit for Soil (MP Biomedicals, USA). DNA underwent PCR, using universal primer pair F515 and R926 (positions 515 to 926 in the V4–V5 region; *Escherichia coli* numbering), which target both Bacteria and Archaea. Forward primers used 'golay_12' barcodes and Torrent adaptor A for identification. Initial denaturation was at 95 °C for 5 min; 30 cycles of 95 °C for 1 min, 55 °C for 1 min, 72 °C for 1 min, and a final elongation step of 72 °C for 10 min. PCRs were performed on a Techne 512 thermocycler, in triplicate. Amplicons were cleaned using Agencourt AMPure XP (Beckman Coulter, USA), quantified via a Qubit 3.0 fluorometer (Life Technologies, USA) and pooled. Sequencing was performed on an Ion Torrent Personal Genome Machine (Thermo Fisher Scientific, USA) on a 316 chip. Sequencing produced reads with a modal length of 481 bases. The average number of reads in individual binned libraries after filtering and OTU phylogenetic assignment filtering was 13,945, ranging from 7766 to 21,844. Libraries were rarefied to 7766 sequences for comparative analysis of sequences. Sequences have been deposited in the NCBI Sequence Read Archive available under the BioProject PRJNA413685. Pipeline analysis was performed using QIIME 1.9.1 (Caporaso et al., 2010), with OTU matching performed at 97% similarity against the SILVA128 reference database (Quast et al., 2013). OTU tables were standardized by total for each sample depth, and square root transformed, in PRIMER 6 (Clarke and Gorley, 2006). Bray Curtis similarity and non-metric Multidimensional Scaling (nMDS) analysis was then performed. Taxa representative of significant changes in redox conditions were then selected and their relative abundances determined.

2.5. X-ray absorption spectroscopy and μ-focus X-ray fluorescence

Select samples (1, 5, 10, 15, 20, 23, 25, 27, and 30 cm) were analyzed by U L_3-edge XAS to determine variation in U oxidation state and coordination environment with depth. Spectra were recorded on beamline B18 at Diamond Light Source, UK and the MARS beamline at Synchrotron Soleil, France. A sub-set of samples (10, 20, 25, and 30 cm) were also analyzed by high energy resolution fluorescence detector X-ray absorption near edge structure (HERFD-XANES) spectroscopy on the U M_4-edge (3728 eV) at beamline ID26 at the European Synchrotron Radiation Facility, France. XAS data collection and processing is detailed in the Appendix (section S4).

Micro-focus X-ray fluorescence maps were also recorded at beamline I18 at Diamond Light Source, UK, from resin-embedded Needle's Eye soil thin-sections. Data collection and processing details are presented in the Appendix (section S1).

3. Results & discussion

3.1. Soil biogeochemistry

The soil collected close to the Needle's Eye pitchblende vein (Fig. S1) was waterlogged (up to 80% water by weight). When dried, the soil was comprised of up to 85% organic matter at the surface and this decreased steadily with depth to a minimum of ~25 wt % at 30 cm (Fig. 1A and Fig. S2). In contrast, the soil Si content increased from 1 wt % at the surface to 22 wt % at 30 cm, reflecting an increasing mineral fraction with depth and suggesting that the decrease in organic matter largely reflects dilution by increasing mineralization. The soil pH was between 6.6 and 7 (Table S2). The soil from the control site was also waterlogged and had a similar texture.

Solid phase Mn and Fe and community analysis of microbes were used to give a time-integrated picture of redox zonation in the soil collected close of the pitchblende vein. Mn and Fe were normalised to Al to help resolve any redox-driven variability with depth (Morford and Emerson, 1999). There was a decrease in Mn/Al between 0 and 12 cm (Fig. 1B) consistent with Mn oxy(hydr)oxide bioreduction. Solid phase Fe (Fig. 1C) showed a similar trend although the Fe/Al ratio was stable down to 10 cm, suggesting that above this depth the system was dominated by Mn reduction and/or other suboxic processes (i.e. N cycling). Around 15 cm there was a ~2/3rd decrease in the Fe/Al ratio, indicative of microbially-mediated Fe(III) reduction (Tribovillard et al., 2006). The Fe/Al ratio then remained stable until around 23 cm and then fell to a minimum at 30 cm. This trend was mirrored by a concurrent increase in groundwater/porewater Fe (Fig. 1F) between 15 and 25 cm, further confirming that the soil system became increasingly reducing with depth. Ferrozine analysis of 0.5 N HCl extracted solid phase Fe was used to provide an estimate of "bioavailable" Fe (Lovley and Phillips, 1987) in the soil (Fig. 1E). Using this assay, ~100% of the extractable Fe was present as Fe(II) in the soil except for a horizon between ~5 and 15 cm, where up to 40% of the extractable Fe was present as Fe(III). A lateral input of more oxidizing groundwater at this depth may account for the changes in 0.5 N HCl extractable Fe between ~5 and 15 cm (Fig. 1E) in the soil profile. Impacts of Fe(II/III) organic complexation on this method are unclear and thus the data should be interpreted with caution.

Microbial community analysis allowed us to further understand the pattern and stability of redox zonation at Needle's Eye. Here, our inferences are based on identification of functionally indicative dominant taxa and an assumption of the typical persistence of microbial DNA on a timescale of weeks to months in soils and sediments (Nielsen et al., 2007). The relative abundance of bacterial and archaeal operational taxonomic units (OTUs) derived from 16S rRNA gene libraries generated at a 1 cm resolution showed two visually discernible zones of community composition separated at 23 cm (confirmed by nMDS analysis; Fig. S3).

Phylogenetic analysis of specific dominant sequence types and their relative abundance profiles indicated the likely importance of aerobic and suboxic processes in the upper 23 cm of the core. Specifically, sequences assigned to ammonia oxidizers *Nitrosomonoadaceae* (Prosser et al., 2014) and *Thaumarchaeota* (Spang et al., 2010; Swan et al., 2014), and the nitrite oxidizer *Nitrospiraceae* (Daims, 2014), were found in this region (Fig. 1H). These sequence types peaked in relative abundances at about 10 cm, centered on the same depth range as maximum 0.5 N HCl

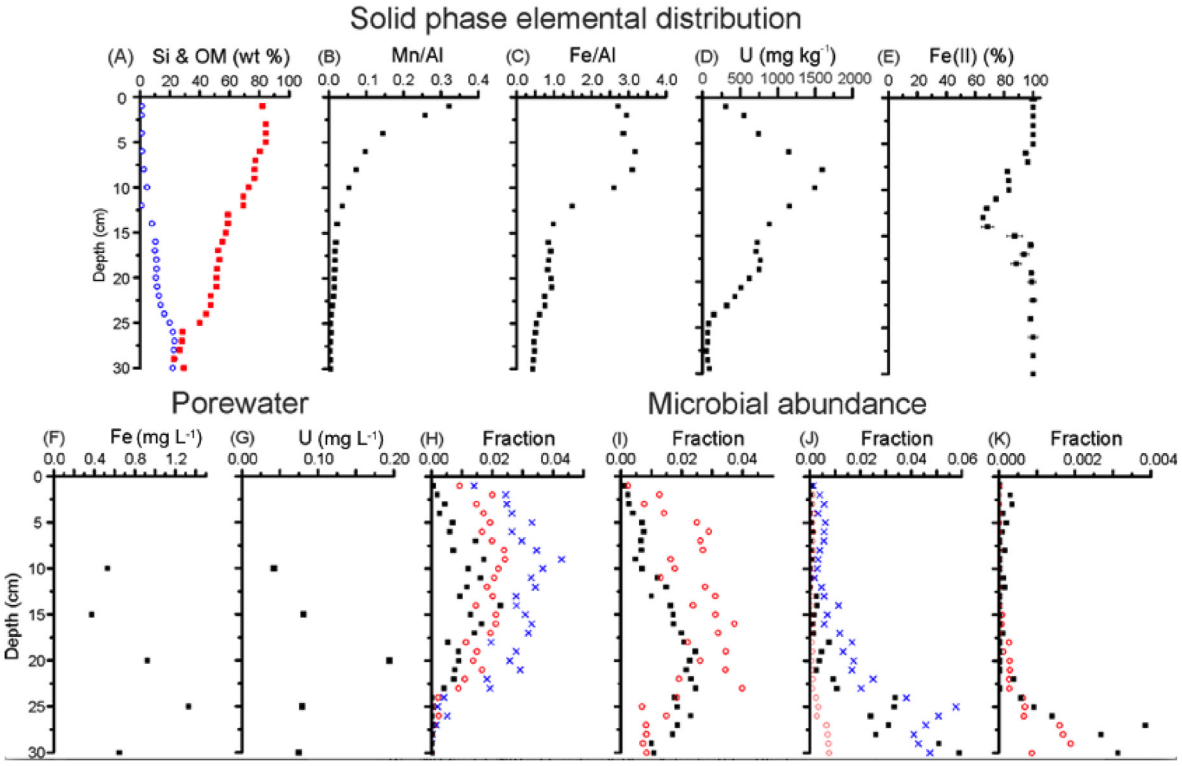

Fig. 1. Sediment: **(A)** Si = ○ and organic matter (OM) = ■ content; **(B)** Mn/Al ratio; **(C)** Fe/Al ratio; **(D)** U concentration; and **(E)** 0.5 N HCl extractable solid phase Fe(II) as a % of total extractable Fe. Groundwater/porewater: **(F)** Fe, and **(G)** U concentrations. Fractional abundance of key taxa: **(H)** nitrite and ammonia oxidizers where ■ = Thaumarchaeota, ○ = Nitrospira, and X = Nitrosomonadaceae; **(I)** sulfide oxidizers and nitrate reducers where ■ = δ-proteobactaeria 43F-1040r and ○ = Sulfurifustis; **(J)** anaerobic methane oxidisers and sulfate reducers where ■ = δ-proteobactaeria Sva0485, ○ = Desulfobacca, and X = Bathyarchaeota, and **(K)** syntrophs and methanogens where ■ = Methanolinea and ○ = Smithella.

extractable Fe(III), but were not detected below 23 cm. Sequences related to the genus *Sulfurifustis* (sulfur oxidizers, originally identified in a nitrate-reducing enrichment; Kojima et al., 2015) were found at similar depths (Fig. 1I) and sequences affiliated with the deltaproteobacterial clade 43f-1404r, associated with nitrate and nitrite reduction to ammonium (Hug et al., 2016), peaked between ~15 and 25 cm (Fig. 1I).

In contrast, the bottom of the core (24–30 cm) was characterized by increasing abundances of strictly anaerobic bacteria and archaea, indicating that the core becomes more reducing at this depth. These strict anaerobes (Fig. 1J) included: the Bathyarchaeota, which are putative anaerobic methane oxidizers (Evans et al., 2015), acetogens, and fermenters of a variety of organic substrates; deltaproteobacteria (specifically, sequences related to the SVa0485 group) and members of the genus *Desulfobacca,* both of which are obligate anaerobic sulfate reducers (Bar-Or et al., 2015). In addition, a deltaproteobacterial sequence related to the genus *Smithella* (fermenters typically only found in the presence of a hydrogen-consuming syntrophic partner; Gray et al., 2011; Kuever, 2014) was enriched between 24 and 30 cm (Fig. 1K). This region was also enriched in the *Methanolinea* (Fig. 1K), which are hydrogenotrophic methanogens (Oren, 2014) known to participate in such syntrophic associations (Wu et al., 2013).

Taken together, the geochemical and microbial community data are consistent with stratification of the core into two discrete redox zones. Down to 23 cm the soil appears to be suboxic, becoming increasingly reduced with depth, as evidenced by the decrease in solid phase Mn and Fe below ~10 and ~15 cm, respectively. Here taxa associated with N-cycling dominate, but oxidizers are also abundant in the region with the highest Fe(III). As previously suggested, this may reflect an inflow of oxidizing groundwater at this depth (~10 cm). Below 23 cm the soil transitions to become sulfidic and even methanogenic. The consistently high organic C percentages indicate low levels of organic matter degradation throughout the core. The inconsistency between high organic matter accumulation and dominantly suboxic conditions suggests the labile C has been rapidly respired and removed from the system and that the remainder of the organic C is relatively refractory.

3.2. Uranium distribution

The "background" soil U concentration (core collected 100 m away from the Needle's Eye pitchblende vein) was <10 mg kg^{-1}. In contrast, U concentrations in the core collected close to the pitchblende vein (Fig. S1) were enriched above this background, attaining a maximum of ~1600 mg kg^{-1} U at 8–10 cm depth (Fig. 1D). Below this depth, the solid-phase U concentrations gradually decreased to a minimum of 47 mg kg^{-1} at 28 cm. Analysis of groundwater/porewater showed the highest aqueous U concentration around 20 cm (0.19 mg L^{-1}, Fig. 1G).

Synchrotron X-ray μ-focus XRF mapping of resin embedded Needle's Eye soil thin-sections was also completed at several depths, and representative maps from ~5 cm and ~26 cm are shown in the Appendix (Fig. S4). At all depths, U was largely found to be co-located with key life elements such as Ca and Zn, indicating possible uptake of U by organic matter. Alternatively, the correlation of U with Ca may indicate association of U with Ca-carbonates. Most notably, XRF mapping of what appeared to be preserved organic material at ~5 cm soil depth showed evidence for high U uptake. In contrast, U co-location with Fe was distinctly lacking in XRF maps except for a few Fe/U enriched areas >25 cm soil depth when the soil became more mineral rich. These findings contrast with other studies that show U co-location and chemical coordination with Fe in both oxic and reducing soils and sediments (e.g. Li et al., 2014, 2015; Bower et al., 2019).

A sequential extraction was performed to probe the dominant phase(s) responsible for the high retention of U on the soil. Extractions were completed on samples from 15 cm, where the soil organic matter and U concentrations were high and the soil was Fe(III)-reducing, and 30 cm, where the soil was more mineral-rich, had lower overall U, and was sulfate-reducing/methanogenic (Fig. 1; Table S3). At both depths the U was found to be concentrated in the acetate extractable 'carbonate' fraction and the H_2O_2 extractable 'organic' fraction. Specifically, at 15 cm, 63% of the U was in the acetate fraction and ~29% in the H_2O_2 fraction. At 30 cm, ~45% was present in the acetate fraction and ~49% in the H_2O_2 fraction (full extraction data is presented in Table S3). Although the acetate extraction is typically used to target carbonate minerals, the moderate pH (6.6–7) of the Needle's Eye soil system and the low total inorganic carbon (<1% in the surface sediments) make it highly unlikely that up to 63% of the U would be associated with carbonates. Additionally, the samples contained negligible dissolved inorganic C (<0.2 mg L^{-1}) in the 'carbonate' fraction, strongly suggesting that this step was not dissolving carbonate minerals. As U readily forms U-acetate complexes (Jiang et al., 2002) it is possible that this extraction step instead reflects the 'acetate exchangeable U' fraction.

To further test whether this fraction indeed reflected acetate exchange rather than carbonate dissolution, we subjected soils from both depths to extraction with 0.001 and 0.1 mol L^{-1} HCl in an attempt to achieve the same desired reduction in pH without the presence of acetate. Here, $\leq$ 0.1% of the U was released into solution at both depths (Table S4). This supports the inference that U extractability seen in the acetate treatment was not occurring as a function of pH change, and was most likely due to U exchange from the soil surface ligands to the acetate ligand in solution, rather than carbonate dissolution.

3.3. Uranium L_3-edge XANES and M_4-edge HERFD-XANES

The solubility and hence mobility of U is typically controlled by its oxidation state. At Needle's Eye, U soil concentrations were highest at 8–10 cm depth (Fig. 1D) where the soil is suboxic. U is usually bio-reduced from U(VI) to U(IV) around the Fe(II)/(III) redox couple, either enzymatically, or through interaction with mineral-bound or biogenic Fe(II) (Newsome et al., 2014). Therefore, it would be expected that the U(IV) would dominate in this soil, given the presence and dominance of Fe(II) throughout the soil (Fig. 1E), and the microbial community transition to sulfate reduction and methanogenesis at depth. To investigate the oxidation state of the U in the Needle's Eye soil, we collected XANES spectra from the U L_3-edge and HERFD-XANES from the U M_4-edge. Firstly, the L_3-edge XANES (Fig. 2A) showed that U(VI) was dominant from 1 to 23 cm. This was evidenced by the presence of the distinctive uranyl shoulder feature (labelled A in Fig. 2A) (also see E_0 and white line energies; Table S5). This feature results from the multiple scattering of the ejected photoelectron between the two axial O atoms in the uranyl moiety. Between 23 and 30 cm, an increasing proportion of the U was present as U(IV), reflected by the decreased amplitude of the uranyl shoulder feature, and a concurrent increase in amplitude at ~17,215 eV (Fig. 2A, feature B) which results from an increased proportion of the O in the U(IV) equatorial plane. The shift in O coordination was accompanied by a decrease in the edge energy (of around 1 eV; Table S5), again indicative of reduction. To quantify the proportions of U(VI) and U(IV), a linear combination fit of the experimental spectra was performed with U(VI) and U(IV) standards (the full L_3-edge XANES results and further details are provided in Table S5). This confirmed that U(VI) was dominant (~80–100% of total U) down to 23 cm depth, with the highest U(VI) (~100%) found alongside the highest U concentration at 10 cm, and

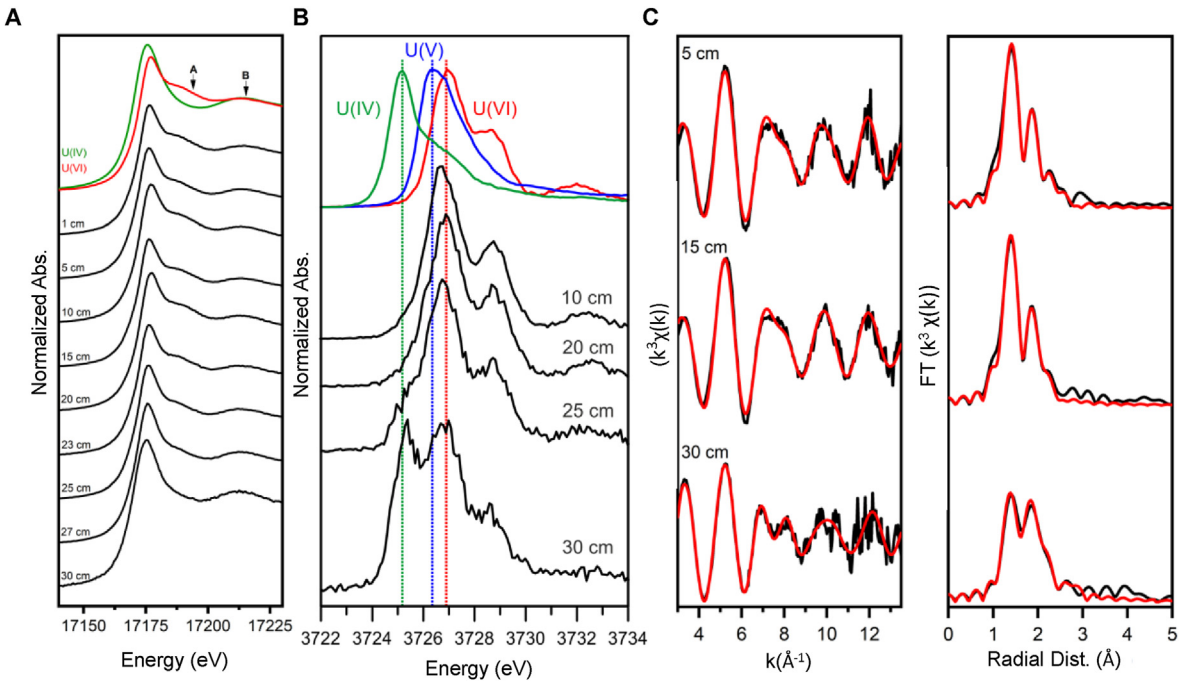

Fig. 2. **(A)** U L_3-edge XANES spectra from samples of different depth. U(VI) and U(IV) standard spectra are provided for comparison and were used in LINCOM modelling (see Table S5 for further detail). For clarity, the U(VI) and U(IV) XANES distinctive structural features are labelled with arrows. A = axial oxygen shoulder feature of uranyl, B = equatorial oxygen feature of U(IV). **(B)** U M_4-edge HERFD-XANES from selected soil depths. U(IV), U(V/VI), and U(VI) standards are provided for comparison and were used in IFTA modelling. Vertical lines mark the edge energies of U in its various oxidation states where green = U(IV), blue = U(V), and red = U(VI). **(C)** U L_3 edge EXAFS data (black) with accompanying best-fits (red) for samples taken at 5, 15, and 30 cm depth. Data presented with accompanying non-phase-shifted Fourier transform. (For interpretation of the references to colour in this figure legend, the reader is referred to the Web version of this article.)

then also at 20 cm. The U(IV) fraction then increased from ~10% at 23 cm to ~66% at 30 cm, indicating that a significant proportion of the U was still present as U(VI) under sulfate reducing conditions.

There is increasing evidence that, as well as the dominant U(VI) and U(IV) oxidation states, U(V) may also be present in the environment. U(V) can be formed through microbial action or abiotic reduction and be stabilized by mineral interaction (e.g. Renshaw et al., 2005; Ilton et al., 2010; Pidchenko et al., 2017; Roberts et al., 2017; Vettese et al., 2020). As it is hard to differentiate between U(V) and U(VI) using standard L_3-edge XANES, we collected HERFD-XANES from the U M_4-edge, where the reduced broadening of the spectral features (compared to the L_3-edge) and the enhanced resolution allows clearer distinction of the different oxidation states (Kvashnina et al., 2013). Fig. 2B shows HERFD-XANES spectra from select samples together with standards of U(IV) (UO_2), U(VI) (UO_3), and U(V/VI) (U_3O_8). Although it has been postulated that U(V) may form in reducing organic soils (Koster van Groos et al., 2016), the Needle's Eye M_4-edge spectra did not show any peak at the U(V) edge energy. The absence of U(V) was confirmed by principal component analysis using the ITFA program (Rossberg et al., 2003). We therefore quantified the concentrations of U(IV/VI) by performing an iterative target test with appropriate standards (UO_2 and UO_3) as end-members of each oxidation state. The outcome of this analysis (Table S6; Fig. 2B) was broadly similar to the L_3-edge data (Table S5; Fig. 2A) and showed that U(VI) was dominant at 10 cm (75%), 20 cm (80%), and 25 cm (60%), whilst U(IV) was dominant (70%) at 30 cm.

Overall, the XANES data show that the accumulation of U in the upper section of the core (above 23 cm) is not dominated by U(VI) reduction. Instead, U(VI) dominates U speciation as deep as 25 cm, despite suboxic conditions in most of the core, and evidence of Fe(III) reduction (Fig. 1). Indeed, U(IV) only becomes prevalent after 25 cm, when the soil system becomes more reducing (as evidenced by the presence of sulfate reducing bacteria and methanogens). However, even here, up to ~34% of the U remained as U(VI). This suggests that the organic soil matrix either sequesters U(VI) in a quasi-stabilized form that is recalcitrant to reduction, or that U(VI) reduction is not favorable for the native microbial community despite suboxic to anoxic conditions throughout the soil system.

3.4. Uranium bonding environment

To better define the U retention mechanism in the Needle's Eye soils, we performed U L_3-edge extended X-ray absorption fine structure (EXAFS) measurements on 3 samples taken from 5 cm, 15 cm, and 30 cm depth in the soil core. The EXAFS spectra, their Fourier transforms, and modelled outputs are shown in Fig. 2C. The corresponding fits are also detailed in Table 1. The 5 cm sample EXAFS was best fit by 3 O shells: 2 O at 1.82 ± 0.01 Å, indicative of

Table 1
EXAFS fitting parameters and statistics for soil samples. Here n = coordination number (shell occupancy), R = interatomic distance, σ2 = Debye-Waller factor, and R factor = least squared residual for the overall fit.

Sample	Atom	n	R (Å)	σ^2 (Å^2)	R-factor
5 cm	O_{ax}	2	1.82 ± 0.01	0.003 ± 0.001	
	O_{eq}	3	2.34 ± 0.02	0.005 ± 0.003	
	O_{eq}	2.5	2.49 ± 0.03	0.005 ± 0.004	
	C	1.5	2.89 ± 0.04	0.004 ± 0.005	0.012
15 cm	O_{ax}	2	1.79 ± 0.01	0.003 ± 0.001	
	O_{eq}	3	2.33 ± 0.03	0.006 ± 0.004	
	O_{eq}	2.5	2.47 ± 0.03	0.006 ± 0.005	
	C	2	2.90 ± 0.05	0.008 ± 0.007	0.014
30 cm	O_{ax}	0.9	1.79 ± 0.01	0.001 ± 0.001	
	O_{eq}	4.0	2.33 ± 0.01	0.007 ± 0.001	
	O_{eq}	4.0	2.49 ± 0.01	0.007 ± 0.001	
	P	2	3.10 ± 0.02	0.007 ± 0.002	0.011

uranyl axial O backscatters, confirming our L_3-edge XANES and M_4-edge HERFD-XANES results, and a split equatorial O shell with 3 O at 2.34 ± 0.02 Å and 2.5 O at 2.49 ± 0.03 Å. The fit was also improved by inclusion of 1.5 C at 2.89 ± 0.04 Å. Fitting minor oscillations beyond 3 Å with P, Si, and Fe shells, and multiple scattering paths was attempted but yielded no statistically significant improvement to the fit. A very similar fit was obtained for the EXAFS data collected from the 15 cm sample (Table 1). Therefore (and informed by the sequential extraction data) it appears that the U(VI) at these depths is predominantly retained by association with soil organic matter. At both depths, the equatorial O coordination numbers and bond distances occur within the ranges identified by Denecke et al. (1997) for bridging (2.36 ± 0.05 Å) and bidentate (2.48 ± 0.05 Å) ligand formation on the carboxylate groups of humics suggesting a mix of these two surface complexes in the Needle's Eye sample. Our U–C distance of ~2.9 Å was also in close agreement with Denecke et al. (1998 A and B) who examined U reaction with organic acids. These results indicate that the U is likely coordinated by carboxylate groups at these depths, which have been previously identified as the primary site of U sorption on organic acids (Schmeide et al., 2003). Mikutta et al. (2016) have previously identified the formation of U bidentate-mononuclear complexes in peats and we extend this model to highlight the importance also of bridging ligands in retaining U(VI) in organic-rich soil.

We also note that an alternative modelling explanation for the 5 and 15 cm EXAFS data could be a U-carbonate type coordination. However, the low acid extractability of soil bound U at these depths (<1%; Table S4) means that relative abundance of U-carbonate species at these depths is likely low. Similarly, the low U concentrations in the $MgCl_2$ exchangeable and oxide sequential extraction fractions (Table S3) indicates that U-carbonate surface complexes on Fe minerals (for example, Bargar et al., 2000) are not significant. Additionally, we were not able to resolve the Fe or Si backscatterers previously modelled for these U-carbonate surface complexes' EXAFS spectra (Bargar et al., 2000).

Sorption and retention of U(VI) in organic-rich soils, or soils artificially amended with plant materials, has been observed by a range of authors (e.g. Bednar et al., 2007; Li et al., 2014; Kaplan et al., 2016; Mikutta et al., 2016; Cumberland et al., 2018B). Interestingly, Ortiz-Bernad et al. (2004) observed that once U(VI) is adsorbed to organic-rich sediments, a significant fraction of the U is not readily bioreducible. In light of this, we suggest that U enrichment at the Needle's Eye site results from: (i) $U(VI)_{(aq)}$ transport into the soil after weathering of the nearby pitchblende vein; (ii) fixation of U(VI) in the soil due to complexation with the organic matter, which likely dominates the reactive surface area of the soil. These U(VI)-organic interactions likely then form strong, reasonably stable U-complexes that limit U from re-entering the site's groundwater.

EXAFS from the 30 cm sample (Fig. 2C, Table 1) was best modelled with a different co-ordination environment. Occupancy of the axial O backscattering shell was reduced to 0.9, indicating that 45% of the U was present as U(VI) (i.e. ~10–15% more than indicated by the L_3-edge XANES and M_4-edge HERFD-XANES (Tables S5 and S6)). It is interesting that U(VI) is still found at this depth and it further indicates that U(VI) organic complexation hinders U(VI) reduction, even under strongly reducing conditions. The presence of U(IV) in the 30 cm sample was then reflected by an increased equatorial O contribution to the EXAFS (Table 1). Assuming that U(VI) has ~6 equatorial oxygens, the fit for the 30 cm sample indicates that an average U(IV) atom would have ~9 coordinating O. The fit for this sample was also statistically improved by the addition of a P shell at ~3.10 Å, but a U–U interaction at ~3.8 Å (indicative of nanocrystalline UO_2; Newsome et al., 2015) could not be modelled. This U(IV) coordination (Table 1) is similar to models for non-crystalline U(IV) species described in the literature (e.g. Bernier-Latmani et al., 2010; Boyanov et al., 2011; Morin et al., 2016). As such, under the sulfate-reducing to methanogenic conditions found at 30 cm depth at Needle's Eye, the majority of the U(IV) appears to be present as non-crystalline U(IV). This is interesting as UO_2 has been found to be the more favorable product of U(VI) reduction over time in a number of studies (e.g. Stylo et al., 2013; Newsome et al., 2015; Bower et al., 2019).

3.5. Uranium availability

The sequential extraction and XAS data showed that U in the Needle's Eye soil was predominantly associated with the organic matrix as U(VI) between 0 and 23 cm, with U(IV) becoming dominant by 30 cm depth. To test how this governs longer-term U retention in the Needle's Eye soil, samples from 15 cm (predominantly U(VI)) and 30 cm (predominantly U(IV)) were reacted for one month with 0.1 M $MgCl_2$ under both oxic and anoxic conditions. The $MgCl_2$ treatment should have targeted readily exchangeable U in the soils, and when completed under oxic conditions, also allowed assessment of the potential for oxidative remobilisation of non-crystalline U(IV) in the 30 cm sample.

Only a negligible amount of U was released to solution from the 15 cm samples after one month (<1% of total available soil U, Fig. 3), and the 30 cm samples showed a comparable U release. The total U release was significantly lower than seen in previous oxidation studies with non-crystalline U(IV), UO_2, or U(IV) containing sediments, where up to 100% of the available U was oxidized and released to solution (e.g. Moon et al., 2007; Law et al., 2011; Campbell et al., 2011; Cerrato et al., 2013; Newsome et al., 2015). Newsome et al. (2015) noted that around 20% of bioreduced U(IV) was recalcitrant to reduction, and Campbell et al. (2011) noted that re-oxidation of U(IV) may be diffusion limited. However, as our systems were agitated and such a large portion of the U remained in the solid phase, neither of these explanations hold for our soil system. It may be that the U(IV) fraction in the 30 cm sample is being retained in such a way that it inhibits oxidation. Alternatively, any U(IV) that is oxidized from the 30 cm samples may be retained by resorption as U(VI) on the organic matter in the sediments, preventing its remobilisation to solution.

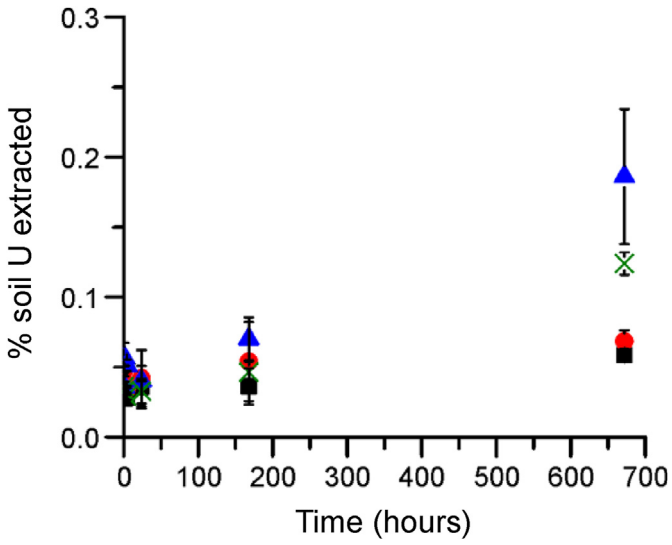

Fig. 3. % of soil U extracted by exchange with 0.1 M $MgCl_2$, from a 15 cm sample (■ = oxygenated, and ● = O_2 free atmosphere) and 30 cm (▲ = oxygenated, and X = O_2 free atmosphere). Error bars 1-sigma from replicate measurements.

4. Conclusions

Our study shows that U enrichment in Needle's Eye soils is predominantly controlled by organic complexation of U(VI), in spite of the suboxic to Fe(III)-reducing conditions that dominate most of the soil profile. Non-crystalline U(IV) only dominated in deeper, sulfidic-to-methanogenic soil but U(VI) was still significant at this depth. We found no evidence of UO_2, as hypothesized for this site, and despite the long equilibration time for U(IV) in the soil. Organically complexed U(VI), and the U(IV) found at 30 cm, also appear to have low chemical availability/leachability. Overall, the lack of U availability at Needle's Eye confirms that soils dominated by refractory organic matter can represent potential long-term sinks for U, irrespective of their redox state. As such, the creation of artificial wetlands, or the use of organic-rich materials in permeable reactive barriers, can be effective options for limiting U migration through the geosphere at contaminated sites (e.g. Groza et al., 2010; Cumberland et al., 2018B). Further, U that is eventually released from radioactive waste geological disposal facilities may be effectively captured by organic-rich soils, limiting potential movement of U through the biosphere.

Credit author statement

AJF, PL, NDG, JFWM, FRL, GL: Study conceptualization, data collection, data processing and interpretation, and manuscript writing. All other authors assisted with data collection, data processing, and/or with editing of the manuscript.

Declaration of competing interest

The authors declare no competing interests.

Acknowledgements

This work was funded as part of the LO-RISE (Long-lived Radionuclides in the Surface Environment; NE/L000202/1) consortium under the UK NERC RATE programme (Radioactivity and the Environment), co-funded by the UK Environment Agency and Radioactive Waste Management Ltd. Synchrotron data was collected at Diamond Light Source on beamline B18 (SP10163 and SP12767), I18 (SP12477), and at the MARS beamline, Synchrotron Soleil (20150125). Law also thanks the UK STFC and NERC for funding through the Environmental Radioactivity Network (ST/K001787/1) and grant NE/M014088/1. We thank Paul Lythgoe and Alastair Bewsher for assistance with geochemical analysis, Dr Stephen Parry, Dr Pier Lorenzo Solari, Dr Akhil Tayal, Herve Hermange, and Richard Doull for assistance with XAS data collection, Dr Hannah Roberts for advice on HERFD-XANES analysis, and Dr Rosemary Hibberd for assistance with sample collection and manuscript proofing. We thank the European Synchrotron Radiation Facility for access to beamline ID26 (20-01-790).

Appendix A. Supplementary data

Supplementary data to this article can be found online at https://doi.org/10.1016/j.chemosphere.2020.126859.

References

Alam, M.S., Cheng, T., 2014. Uranium release from sediment to groundwater: influence of water chemistry and insights into release mechanisms. J. Contam. Hydrol. 164, 72–87.
Alessi, D.S., et al., 2012. Quantitative separation of monomeric U(IV) from UO2 in products of U(VI) reduction. Environ. Sci. Technol. 46, 6150–6157.
Alessi, D.S., et al., 2014. The product of microbial uranium reduction includes multiple species with U(IV)-phosphate coordination. Geochem. Cosmochim. Acta 131, 115–127.
Bar-Or, I., et al., 2015. Methane-related changes in prokaryotes along geochemical profiles in sediments of Lake Kinneret (Israel). Biogeosciences 12, 2847–2860.
Bargar, J.R., et al., 2013. Uranium redox transition pathways in acetate-amended sediments. Proc. Natl. Acad. Sci. Unit. States Am. 110, 4506–4511.
Bargar, J.R., et al., 2000. Characterization of U(VI)-carbonato ternary complexes on hematite: EXAFS and electrophoretic mobility measurements. Geochem. Cosmochim. Acta 64, 2737–2749.
Bednar, A.J., et al., 2007. Effects of organic matter on the distribution of uranium in soil and plant matrices. Chemosphere 70, 237–247.
Bernier-Latmani, R., et al., 2010. Non-uraninite products of microbial U(VI) reduction. Environ. Sci. Technol. 44, 9456–9462.
Bone, S.E., et al., 2017. Uranium(IV) adsorption by natural organic matter in anoxic sediments. Proc. Natl. Acad. Sci. Unit. States Am. 114, 711–716.
Bower, W.R., et al., 2019. Metaschoepite dissolution in sediment column systems-Implications for uranium speciation and transport. Environ. Sci. Technol. 53, 9915–9925.
Boyanov, M.I., et al., 2011. Solution and microbial controls on the formation of reduced U(IV) species. Environ. Sci. Technol. 45, 8336–8344.
Campbell, K.M., et al., 2011. Composition, stability, and measurement of reduced uranium phases for groundwater bioremediation at Old Rifle. CO. *Appl. Geochem.* 26, 167–169.
Caporaso, J.G., et al., 2010. QIIME allows analysis of high-throughput community sequencing data. Nat. Methods 7, 335–336.
Catalano, J.G., Brown Jr., G.E., 2005. Uranyl adsorption onto montmorillonite: evaluation of binding sites and carbonate complexation. Geochem. Cosmochim. Acta 69, 2995–3005.
Cerrato, J.M., et al., 2013. Relative reactivity of biogenic and chemogenic uraninite and biogenic noncrystalline U(IV). Environ. Sci. Technol. 47, 9756–9763.
Choppin, G., et al., 2002. Behavior of radionuclides in the environment. In: Radiochemistry and Nuclear Chemistry, third ed., pp. 653–685.
Clarke, K.R., Gorley, R.N., 2006. PRIMER V6: User Manual/Tutorial. PRIMER-E.
Cumberland, S.A., et al., 2016. Uranium mobility in organic matter-rich sediments: a review of geological and geochemical processes. Earth Sci. Rev. 159, 160–185.
Cumberland, S.A., et al., 2018 A. Characterization of uranium redox state in organic-rich Eocene sediments. Chemosphere 194, 602–613.
Cumberland, S., et al., 2018 B. Rapid immobilisation of U(VI) by Eucalyptus bark: adsorption without reduction. Appl. Geochem. 96, 1–10.
Daims, H., 2014. The family Nitrospiraceae. In: Rosenberg, Eugene, et al. (Eds.), The Prokaryotes: Other Major Lineages of Bacteria and the Archaea, pp. 733–749.
Denecke, M.A., et al., 1997. Measurements of the structural parameters for the interaction of uranium(VI) with natural and synthetic humic acids using EXAFS *radiochim.* Acta 79, 151–159.
Denecke, M.A., et al., 1998 A. Determination of structural parameters of uranyl ions complexed with organic acids using EXAFS. J. Alloys Compd. 271–273, 123–127.
Denecke, M.A., et al., 1998 B. EXAFS investigations of the interaction of humic acids and model compounds with uranyl cations in solid complexes. Radiochim. Acta 82, 103–108.
Evans, P.N., et al., 2015. Methane metabolism in the archaeal phylum Bathyarchaeota revealed by genome-centric metagenomics. Science 350, 434.
Fletcher, K.E., et al., 2010. U(VI) reduction to mononuclear U(IV) by desulfitobacterium species. Environ. Sci. Technol. 44, 4705–4709.
Gray, N.D., et al., 2011. The quantitative significance of Syntrophaceae and syntrophic partnerships in methanogenic degradation of crude oil alkanes. Environ. Microbiol. 13, 2957–2975.
Groza, N., et al., 2010. Uranium wastewater treatment using wetland system. Rev. Chim. (Bucharest) 61, 680–684.
Hooker, P., 1991. The geology, hydrogeology and geochemistry of the Needle's Eye natural analogue site. CEC Report 23011032.
Hsi, C.D., Langmuir, D., 1985. Adsorption of uranyl onto ferric oxyhydroxides: application of the surface complexation site-binding model. Geochem. Cosmochim. Acta 49, 1931–1941.
Hug, L.A., et al., 2016. Critical biogeochemical functions in the subsurface are associated with bacteria from new phyla and little studied lineages. Environ. Microbiol. 18, 159–173.
International Atomic Energy Agency, 1989. Natural analogues in performance Assessments for the disposal of long-lived radioactive wastes. Tech. Rep. 304.
Ilton, E.S., et al., 2010. Influence of dynamical conditions on the reduction of U(VI) at the Magnetite–Solution interface. Environ. Sci. Technol. 44, 170–176.
Jamet, P., et al., 1993. Hydrogeochemical modelling of an active system of uranium fixation by organic soils and sediments (Needle's Eye, Scotland). Miner. Deposita 28, 66–76.
Jiang, J., et al., 2002. Complexation of uranium(VI) with acetate at variable temperatures. J. Chem. Soc. Dalton Trans. 8, 1832–1838.
Kaplan, D.I., et al., 2016. Unique organic matter and microbial properties in the rhizosphere of a wetland soil. Environ. Sci. Technol. 50, 4169–4177.
Kojima, H., et al., 2015. Sulfurifustis variabilis gen. nov., sp. nov., a sulfur oxidizer isolated from a lake, and proposal of Acidiferrobacteraceae fam. nov. and Acidiferrobacterales ord. nov. Int. J. Syst. Evol. Microbiol. 65, 3709–3713.
Koster van Groos, P.G., et al., 2016. Uranium fate in wetland mesocosms: effects of plants at two iron loadings with different pH values. Chemosphere 163, 116–124.
Kuever, J., 2014. In: Rosenberg, E., et al. (Eds.), The Prokaryotes: Deltaproteobacteria and Epsilonproteobacteria, pp. 281–288.

Kvashnina, K.O., et al., 2013. Chemical state of complex uranium oxides. Phys. Rev. Lett. 111, 253002.
Law, G.T.W., et al., 2011. Uranium redox cycling in sediment and biomineral systems. Geomicrobiol. J. 28, 497–506.
Li, D., et al., 2014. Retention and chemical speciation of uranium in an oxidized wetland sediment from the Savannah River Site. J. Environ. Radioact. 131, 40–46.
Li, D., et al., 2015. Spectroscopic evidence of uranium immobilization in acidic wetlands by natural organic matter and plant roots. Environ. Sci. Technol. 49 (5), 2823–2832.
Lovley, D.R., Phillips, E.J.P., 1987. Rapid assay for microbially reducible ferric iron in aquatic sediments. Appl. Environ. Microbiol. 53, 1536–1540.
Lovley, D.R., Phillips, E.J.P., 1992. Reduction of uranium by Desulfovibrio desulfuricans. Appl. Environ. Microbiol. 58, 850–856.
Lovley, D.R., et al., 1991. Microbial reduction of uranium. Nature 350, 413–416.
Mackenzie, A.B., et al., 1991. Natural decay series radionuclide studies at the Needle's Eye natural analogue site. British Geological Survey, Tech. Rep. 23002579, 1986-1989.
Mikutta, C., et al., 2016. Tetra- and hexavalent uranium forms bidentate-mononuclear complexes with particulate organic matter in a naturally uranium-enriched peatland. Environ. Sci. Technol. 50, 10465–10475.
Moon, H.S., et al., 2007. Uranium reoxidation in previously bioreduced sediment by dissolved oxygen and nitrate. Environ. Sci. Technol. 41, 4587–4592.
Morford, J.L., Emerson, S., 1999. The geochemistry of redox sensitive trace metals in sediments. Geochem. Cosmochim. Acta 63, 1735–1750.
Morin, G., et al., 2016. Mononuclear U(IV) complexes and ningyoite as major uranium species in lake sediments. Geochem. Persp. Let. 2, 95–105.
Newsome, L., et al., 2014. The biogeochemistry and bioremediation of uranium and other priority radionuclides. Chem. Geol. 363, 164–184.
Newsome, L., et al., 2015. The stability of microbially reduced U(IV); impact of residual electron donor and sediment ageing. Chem. Geol. 409, 125–135.
Nielsen, K.M., et al., 2007. Release and persistence of extracellular DNA in the environment. Environ. Biosaf. Res. 6, 37–53.
Oren, A., 2014. In: Rosenberg, E., et al. (Eds.), The Prokaryotes: Other Major Lineages of Bacteria and the Archaea, pp. 195–199.
Ortiz-Bernad, I., et al., 2004. Resistance of solid-phase U(VI) to microbial reduction during in situ bioremediation of uranium-contaminated groundwater. Appl. Environ. Microbiol. 70, 7558–7560.
Pidchenko, I., et al., 2017. Uranium redox transformations after U(VI) coprecipitation with magnetite nanoparticles. Environ. Sci. Technol. 51, 2217–2225.
Prosser, J.I., et al., 2014. In: Rosenberg, E., et al. (Eds.), The Prokaryotes: Alphaproteobacteria and Betaproteobacteria, pp. 901–918.
Quast, C., et al., 2013. The SILVA ribosomal RNA gene database project: improved data processing and web-based tools. Nucleic Acids Res. 41, 590–596.
Ray, A.E., et al., 2011. Evidence for multiple modes of uranium immobilization by an anaerobic bacterium. Geochem. Cosmochim. Acta 75, 2684–2695.
Regenspurg, S., et al., 2010. Speciation of naturally-accumulated uranium in an organic-rich soil of an alpine region (Switzerland). Geochem. Cosmochim. Acta 74, 2082–2098.
Renshaw, J.C., et al., 2005. Bioreduction of uranium: environmental implications of a pentavalent intermediate. Environ. Sci. Technol. 39, 5657–5660.
Roberts, H.E., et al., 2017. Uranium(V) incorporation mechanisms and stability in Fe(II)/Fe(III) (oxyhydr)Oxides. Environ. Sci. Technol. Lett. 4 (10), 421–426.
Rossberg, A., et al., 2003. Complexation of uranium(VI) with protocatechuic acid—application of iterative transformation factor analysis to EXAFS spectroscopy. Anal. Bioanal. Chem. 376, 631–638.
Schmeide, K., et al., 2003. Interaction of uranium(VI) with various modified and unmodified natural and synthetic humic substances studied by EXAFS and FTIR spectroscopy. Inorg. Chim. Acta. 351, 133–140.
Sharp, J.O., et al., 2011. Uranium speciation and stability after reductive immobilization in aquifer sediments. Geochem. Cosmochim. Acta 75, 6497–6510.
Sherman, D.M., et al., 2008. Surface complexation of U(VI) on goethite (α-FeOOH). Geochem. Cosmochim. Acta 72, 298–310.
Spang, A., et al., 2010. Distinct gene set in two different lineages of ammonia-oxidizing archaea supports the phylum Thaumarchaeota. Trends Microbiol. 18, 331–340.
Stylo, M., et al., 2013. Biogeochemical controls on the product of microbial U(VI) reduction. Environ. Sci. Technol. 47, 12351–12358.
Swan, B.K., et al., 2014. Genomic and metabolic diversity of Marine Group I Thaumarchaeota in the mesopelagic of two subtropical gyres. PloS One 9, e95380.
Tribovillard, N., et al., 2006. Trace metals as paleoredox and paleoproductivity proxies: an update. Chem. Geol. 232, 12–32.
Vandenhove, H., et al., 2014. Comparison of two sequential extraction procedures for uranium fractionation in contaminated soils. J. Environ. Radioact. 137, 1–9.
Vettese, G., et al., 2020. Multiple lines of evidence identify U(V) as a key intermediate during U(VI) reduction by shewanella oneidensis MR1. Environ. Sci. Technol. https://doi.org/10.1021/acs.est.9b05285.
Wang, Y., et al., 2013. Mobile uranium(IV)-bearing colloids in a mining-impacted wetland. Nat. Comms. 4.
Wu, J.-H., et al., 2013. Community and proteomic analysis of methanogenic consortia degrading terephthalate. Appl. Environ. Microbiol. 79, 105–112.
Zimmerman, A.J., Weindorf, D.C., 2010. Heavy metal and trace metal analysis in soil by sequential extraction: a review of procedures. Int. J. Anal. Chem. 2010, 1–7.